Energy Detection Performance with Massive Arrays for Personal Radars Applications

Francesco Guidi[1,2(✉)], Anna Guerra[3], Antonio Clemente[1,2], Davide Dardari[3], and Raffaele D'Errico[1,2]

[1] CEA, LETI, MINATEC Campus, 38054 Grenoble, France
{francesco.guidi,antonio.clemente,raffaele.derrico}@cea.fr
[2] Univ. Grenoble-Alpes, 38000 Grenoble, France
[3] DEI, University of Bologna, Via Venezia 52, 47521 Cesena, Italy
{anna.guerra3,davide.dardari}@unibo.it

Abstract. The idea to adopt massive arrays for personal radars applications is facing a rapid growth, thanks to the high scanning resolution achievable with the large number of antennas employed. In fact, such multi-antenna systems enable the possibility to detect and localize surrounding objects through an accurate beamforming procedure. In this paper we show a classical energy-detection approach for target ranging and localization, where the threshold is designed according to the receiver noise only, since an ideal laser-beam antenna is considered. Successively, we show the ambiguities that could arise when the presence of side-lobes cannot be neglected (e.g., when considering real massive arrays instead of ideal pencil-beam like radiation patterns) and we propose a set of guidelines that can be followed from a system design point-of-view to overcome this issue.

Keywords: Massive arrays · Personal radar · Target detection · Side-lobes

1 Introduction

The adoption of massive arrays is facing a rapid growth in several ranging and localization applications, such as personal radars [1], thanks to the possibility to achieve a precise and high-scanning resolution given by the large number of adopted antennas [2].

The concept of personal radar has been recently proposed in [1,3] where it has been shown the possibility to jointly use millimeter-waves (mmW) and wideband massive arrays technologies for indoor environment mapping. Thanks to this technology, it is possible to avoid the adoption of a dedicated very high-directional antenna with mechanical steering, as proposed in [4–6], which can not be easily integrated into portable radar devices. The consequent near-pencil beam of massive arrays returns a precise angle and range information thus making the modeling and characterization of the environment with personal radars very similar to that based on laser.

D. Noguet et al. (Eds.): CROWNCOM 2016, LNICST 172, pp. 630–641, 2016.
DOI: 10.1007/978-3-319-40352-6_52

Different literature has been produced for the analysis of the localization performance of wideband large antenna arrays. In fact, wideband signals are the best candidate to achieve high ranging performance [7], but a strict phase control in beamforming, i.e. the adoption of precise and costly phase shifters and delay lines, becomes necessary to assure a perfect signal alignment. A cheaper and alternative solution is to adopt digitally controlled phase shifters implementing a discrete set of phase shifts at the price of a reduced signal alignment and an increased level of side-lobes [8,9]. Despite the high-ranging accuracy which can be achieved by the adoption of such systems, all these effects have to be accounted for when target detection is performed for different steering directions.

In this paper we propose a low-complexity non-coherent detection scheme, where the detection of objects is performed by a massive array which steers its beam in different directions in order to detect and localize objects. Thanks to the near-pencil beam array considered, all the measured contributions are associated to the considered steering direction. According to the receiver performance, we describe a set of guidelines to be followed when energy detection with massive arrays is performed.

The rest of the paper is organized as follows. In Sect. 2 we first show the threshold design, and successively we evaluate the side-lobe effects when the previously defined threshold based on receiver noise is adopted. Finally, in Sect. 3 we report a case study where real massive arrays are considered, and we discuss a possible solution to overcome the issue when energy detection is performed.

2 Target Detection Scheme

The personal radar concept is based on the idea that the surrounding objects are detected and localized thanks to the beamforming procedure enabled by massive arrays.

The system herein considered exploits monostatic scattering, i.e. the transmitter and receiver are co-located. For each steering direction θ_b, the massive array steers its main beam towards that direction, and collects the overall backscattered response in order to detect and localize objects. To our purpose, first we account for a laser-like antenna, with a radiation pattern that permits to neglect the side-lobes effect, and thus, we adopt a classical constant false alarm rate (CFAR) approach accounting for the receiver noise only. Second, we focus our analysis to real antennas in which side lobes might cause false target detection. In fact, the presence of a target could be detected and assigned in a certain direction even if it is not effectively located in that part, as shown in Fig. 1. In addition, they could even cause errors in the ranging procedure, i.e. the distance of target 1 and 2 of Fig. 1 can be confused. Thus, once the threshold has been set, we theoretically evaluate the impact of real massive arrays on the detection performance. For our specific case, we consider massive arrays at 60 GHz which can be considered a natural candidate for personal radars applications due to their radiation characteristics.

In the following we describe the receiver scheme considered, and the threshold design by accounting for an ideal laser-beam antenna.

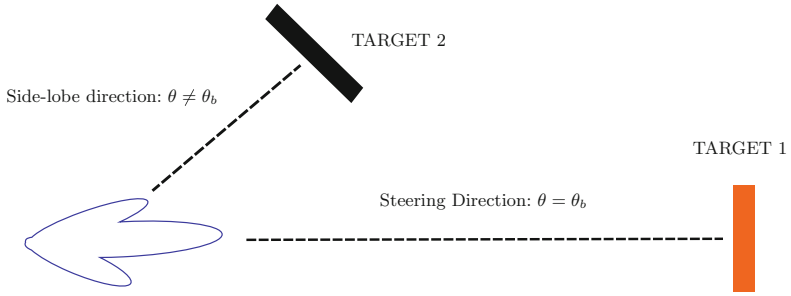

Fig. 1. Considered scenario, where for a steering direction θ_b, the signal reflected from a target in the side-lobe direction is collected.

2.1 Receiver Scheme

The detection scheme we propose is a non-coherent approach based on energy detection to account for the complete uncertainty we have on the received waveform shape.

For each steering direction θ_b, define the received signal as

$$r(t, \theta_b) = s(t, \theta_b) + n(t) \tag{1}$$

with $n(t)$ indicating the noise term and $s(t, \theta_b)$ the received waveform including all the signals coming from the steering direction θ_b.

The received signal is first passed through an ideal bandpass filter with center frequency f_c to eliminate out-of-band noise.[1] The filtered signal is denoted by

$$y(t, \theta_b) = x(t, \theta_b) + z(t) \tag{2}$$

where $x(t, \theta_b) = s(t, \theta_b) \otimes h_F(t)$ and $z(t) = n(t) \otimes h_F(t)$ with $h_F(t)$ being the impulse response of the filter.

Energy evaluations are performed over time interval T_{ED}, with $N_{bin} = \lfloor T_f / T_{ED} \rfloor$ representing the number of integration bins each time frame T_f is divided in, that is

$$e_m(\theta_b) = \int_{(m-1)\,T_{ED}}^{m\,T_{ED}} [y(t, \theta_b)]^2 \, dt \tag{3}$$

with $m = 1, \ldots, N_{bin}$. The detection strategy consists in comparing each element $e_m(\theta_b)$ with a threshold ξ_m. If the energy value of at least one bin is above the threshold, then the target is detected and it is assumed present in the steering direction $\theta = \theta_b$.

We define the following two figures of merit: (i) the probability of false alarm (PFA) P_{FA} as the probability of deciding that a target is detected, when it is not effectively within the considered scenario, due to presence of receiver noise;

[1] This operation is necessary since the receiver is energy-based.

(ii) the crossing probability P_c as the probability that the threshold is overcome due to the signal backscattered from a target placed in the scenario.

If the threshold is exceeded for $m = \hat{m}$, the coordinate $\hat{m}$ leads to an estimate of the target time-of-arrival (TOA) and, jointly with the steering direction θ_b, it provides the spatial position of the target in surrounding environment. Consider now the elements $e_m(\theta_b)$ of the decision energy bins. The presented decision rule consists in

$$\text{Decide}: \begin{cases} \widehat{\mathcal{H}}_0\,, & \text{if } e_m(\theta_b) < \xi_m \quad \forall\{m\}\,, \\ \widehat{\mathcal{H}}_1\,, & \text{if } \exists\,\{m\} \quad \text{s.t.} \quad e_m(\theta_b) \geq \xi_m\,. \end{cases} \tag{4}$$

Define now, for each energy bin, the normalized energy detector test

$$\Lambda_m(\theta_b) = \frac{2}{N_0} e_m(\theta_b) \underset{\widehat{\mathcal{H}}_0}{\overset{\widehat{\mathcal{H}}_1}{\gtrless}} \tilde{\xi}_m \tag{5}$$

where $\tilde{\xi}_m = \frac{N_0}{2}\xi_m$. According to [10] we have

$$\Lambda_m(\theta_b) = \frac{2}{N_0} \int_{(m-1)\,T_{\text{ED}}}^{m\,T_{\text{ED}}} [y(t,\theta_b)]^2\; dt \simeq \frac{1}{\sigma^2} \sum_{i=(m-1)N}^{mN} [y_i(\theta_b)]^2 \tag{6}$$

where $N = 2WT_{\text{ED}}$, $\sigma^2 = N_0 W$ is the noise variance, and y_i are the sampling expansion coefficient of the equivalent low-pass (ELP) of $y(t)$ [10], taken at Nyquist rate W in each interval T_{ED}.

2.2 Threshold Evaluation Criteria with Ideal Pencil-Beam Pattern

When an ideal pencil-beam antenna is considered, we aim to preserve that the probability of false alarm (PFA) due to the receiver noise does not exceed a certain value. Thus, in the presence of only the noise, i.e. $y(t,\theta_b) = z(t)$, Eq. (5) can be written as

$$\Lambda_m(\theta_b) = \frac{2}{N_0} \int_{(m-1)\,T_{\text{ED}}}^{m\,T_{\text{ED}}} [z(t)]^2\; dt \simeq \frac{1}{\sigma^2} \sum_{i=(m-1)N}^{mN} (z_i)^2\,. \tag{7}$$

In order to set the threshold, it is well known that the output of the energy detector is distributed according to a central Chi-square distribution, with probability density function (PDF)

$$f_{\text{C}}(\alpha,\beta) = \frac{\alpha^{(\frac{\beta}{2}-1)}}{2^{\frac{\beta}{2}}\Gamma\left(\frac{\beta}{2}\right)} e^{-\frac{\alpha}{2}}\,, \quad \alpha \geq 0 \tag{8}$$

where $\Gamma(\cdot)$ is the gamma function [11, p. 255] and β is the number of degrees of freedom.

Considering (8), a threshold-crossing event at the mth bin, that is, $\Lambda_m(\theta_b) > \tilde{\xi}_m$, results in a single-bin $p_{\mathrm{FA}}^{(m,b)}$ given by [12]

$$p_{\mathrm{FA}}^{(m,b)} = \tilde{\Gamma}\left(\frac{N}{2}, \frac{\tilde{\xi}_m}{2}\right) \tag{9}$$

with $\tilde{\Gamma}$ denoting the regularized Gamma function [13].

To properly set the threshold, the joint false alarms for all bins have to be taken into account. Thus, for a considered steering direction θ_b, the overall desired false alarm probability is given by

$$P_{\mathrm{FA}}^{\star} = 1 - \prod_{m=1}^{N_{\mathrm{bins}}} \left(1 - p_{\mathrm{FA}}^{(m,b)}\right) \approx N_{\mathrm{bins}} \cdot p_{\mathrm{FA}} \tag{10}$$

where we have assumed that all bins are statistically independent and $p_{\mathrm{FA}}^{(m,b)} = p_{\mathrm{FA}} \ \forall m$, and consequently we can set a desired $p_{\mathrm{FA}}^{\star}$ per bin as

$$p_{\mathrm{FA}}^{\star} \approx \frac{P_{\mathrm{FA}}^{\star}}{N_{\mathrm{bins}}}\,. \tag{11}$$

Finally we can write

$$\tilde{\xi} = 2\left[\mathrm{Inv}\tilde{\Gamma}\left(\frac{N}{2}, \frac{P_{\mathrm{FA}}^{\star}}{N_{\mathrm{bins}}}\right)\right] \tag{12}$$

where $\mathrm{Inv}\tilde{\Gamma}(\cdot,\cdot)$ is the inverse gamma regularized function. Note that with such approach, the threshold does not depend on the bin index, and it is set to keep the probability of false alarm (PFA) due to the receiver noise to a desired value $P_{\mathrm{FA}}^{\star}$.

2.3 Side-Lobes Effects in Energy Detection Schemes

The previous threshold has been set according to a central Chi-square distribution, having accounted for the presence of the noise receiver only. On the contrary, during the steering procedure, in real scenarios we associate all the contributions deriving from the antenna pattern to that of the steering direction θ_b.

This approximation is often incorrect, especially when real arrays are adopted, as shown in Fig. 2. Thus, in order to evaluate the impact of the side-lobes in the target detection performance, we evaluate the probability that the threshold is crossed due to the presence of a target in the side-lobe direction. In particular, define $x(t,\theta_b) = x_{\mathrm{sl}}(t,\theta_b)$ the received backscattering response under the assumption that no target is in the steering direction θ_b, i.e. the target 1 of Fig. 1 is not present. The new random variable (RV) is now distributed as a non-central Chi-square distribution

$$f_{\mathrm{NC}}(\alpha,\lambda,\beta) = \frac{1}{2}e^{-\frac{\alpha+\lambda}{2}}\left(\frac{\alpha}{\lambda}\right)^{\frac{\beta-2}{4}} I_{\frac{\beta}{2}-1}(\sqrt{\alpha\lambda})\,, \quad \alpha \geq 0 \tag{13}$$

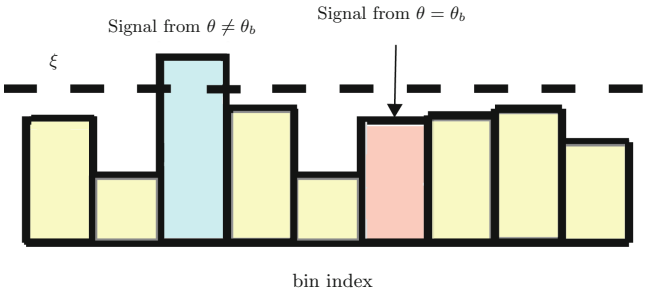

Fig. 2. Example of energy detector output, where energy-bins are compared with the threshold and might cause errors in the localization procedure.

where $I_\kappa(\cdot)$ denotes the κth order modified Bessel function of the first kind [11, p. 374] and probability density function (PDF) $f_{\mathrm{NC}}(\alpha, \lambda, \beta)$ [10], with β being the number of degrees of freedom and λ the non-centrality parameter (NCP).

Due to the presence of signals coming from side-lobes direction, the normalized decision variable results into

$$\Lambda_m(\theta_b) = \frac{2}{N_0} \int_{(m-1)\,T_{\mathrm{ED}}}^{m\,T_{\mathrm{ED}}} \left[x_{\mathrm{sl}}(t, \theta_b) + z(t)\right]^2 \, dt \simeq \frac{1}{\sigma^2} \sum_{i=(m-1)N}^{mN} \left(x_{\mathrm{sl}i}(\theta_b) + z_i\right)^2 \tag{14}$$

where $x_{\mathrm{sl}i}(\theta_b)$ are the sampling expansion coefficients of the equivalent low-pass (ELP) of $x_{\mathrm{sl}}(t, \theta_b)$ [10]. In particular, the presence of $x_{\mathrm{sl}i}(\theta_b)$ leads to the non-centrality parameter (NCP) $\lambda_m(\theta_b) = 2\gamma_m(\theta_b)$ [10,14], where $\gamma_m(\theta_b)$ is the side-lobe-level-to-noise ratio (SLLNR) per bin, given by

$$\gamma_m(\theta_b) = \frac{1}{N_0} \int_{(m-1)\,T_{\mathrm{ED}}}^{m\,T_{\mathrm{ED}}} x_{\mathrm{sl}}(t, \theta_b)^2 \, dt \simeq \frac{1}{2\sigma^2} \sum_{i=(m-1)N}^{mN} \left[x_{\mathrm{sl}i}(\theta_b)\right]^2 \, . \tag{15}$$

A threshold-crossing event at the mth bin, that is, $\Lambda_m(\theta_b) > \tilde{\xi}_m$, results in a single-bin $p_c^{(m,b)}$ given by [12]

$$p_c^{(m,b)} = Q_h\left(\sqrt{\lambda_m(\theta_b)}, \sqrt{\tilde{\xi}_m}\right) \tag{16}$$

with $Q_h(\alpha, \beta) = \int_\beta^\infty x \left(\frac{x}{\alpha}\right)^{k-1} \exp\left(-\frac{x^2+\alpha^2}{2}\right) I_{k-1}(\alpha x)\, dx$ denoting the generalized Marcum's Q function of order $h = \beta/2$ [13].

Since the signals components deriving from side-lobes direction are undesired, we aim that the threshold is not exceeded due to such signals, i.e. $p_c^{(m,b)} \leq p_{\mathrm{FA}}^\star$. If it is not the case, target detection and ranging could be wrongly performed. In the following, the impact of real antenna patterns on the detection performance is investigated, and possible solutions to counteract such effect are reported.

3 Case Study

We now consider the previously described system in order to evaluate what happens when real antennas are employed instead of ideal laser-beam antennas, which are accounted for the threshold design. Despite the analysis conducted is general, i.e. it can be applied to any frequency bandwidth, here we focus on millimeter-waves (mmW) massive arrays, which could be one of the next fifth generation (5G) key technologies. This choice leads to an effective radiated isotropic power (EIRP) constrained by Federal Communications Commission (FCC) regulations as described in [15]. Thus, we first report threshold values in order to achieve a desired $P_{\text{FA}}^{\star}$ based on the receiver noise only. Once the threshold has been defined, we evaluate the bin-crossing probability for different values of the non-centrality parameter (NCP), and finally we evaluate possible values in practical scenarios.

3.1 Threshold Setting

According to the analysis of Sect. 2, we now evaluate the threshold considering the receiver noise level. In particular, if otherwise indicated, we consider a time frame $T_{\text{f}} = 100\,\text{ns}$, a bandwidth $W = 1\,\text{GHz}$ and a time integration interval $T_{\text{ED}} = 1\,\text{ns}$.[2] In this way, by setting an overall $P_{\text{FA}}^{\star} = 10^{-3}$, it is $p_{\text{FA}}^{\star} = 10^{-5}$ which gives the threshold $\tilde{\xi}^{\star}$ reported in Fig. 3. What it is important to remark is that such desired normalized threshold has been set according to the noise receiver only. Consequently, the impact of signals deriving from side-lobe directions has to be evaluated.

3.2 Side-Lobes Effects

When realistic antennas are adopted, and targets outside the steering direction are present, the threshold might be overcome. Consequently, such targets are wrongly associated with θ_b, which translates into a possible detection and localization error. Thus, by considering (16), it is possible to estimate such effects when $\lambda_m(\theta_b)$ is greater than 0.

In particular, we considered in (16), the $\xi^{\star}$ obtained in Fig. 3 in order to preserve an overall $P_{\text{FA}}^{\star} = 10^{-3}$. The obtained results are reported in Fig. 4, where it is evicenced that for $\lambda_m(\theta_b) < 0.2$, the single bin $p_{\text{c}}^{(m,b)}$ is still close to the desired value of 10^{-5}. On the contrary, if we account for $\lambda_m(\theta_b) \approx 2.25$, it is even $p_{\text{c}} = 10^{-3} = P_{\text{FA}}^{\star}$. Obviously, for such values of $\lambda_m(\theta_b)$, the system is not robust for target detection in θ_b, as it is extremely sensitive to the presence of a target outside the desired direction.

In the following, we try to map generic values of the non-centrality parameter (NCP) $\lambda_m(\theta_b)$ to those which can be obtained when massive arrays, as the ones described in [3], are adopted in practical applications.

[2] From [16], the threshold is accurate for large values of N, whereas for low $W\,T_{\text{ED}}$ values, approximations could improve the accuracy of the threshold. Here we kept $N = 2\,W\,T_{\text{ED}}$ since the effects do not affect the validity of the analysis.

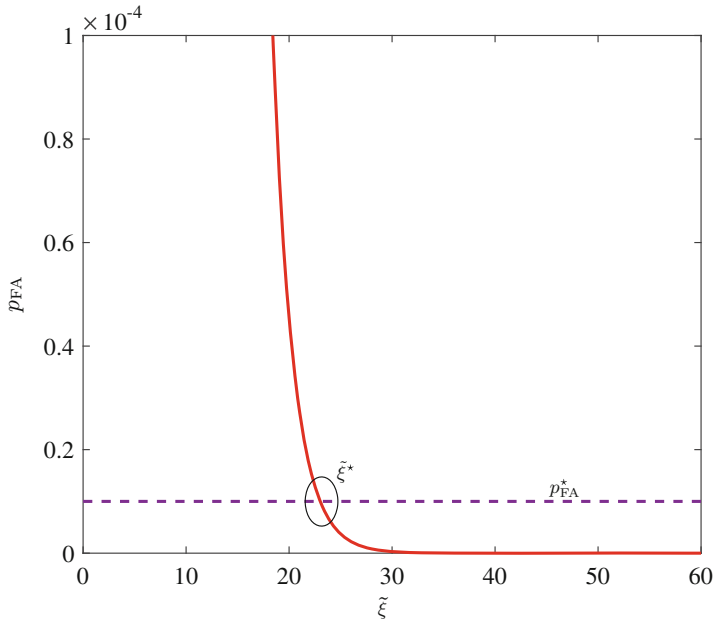

Fig. 3. Threshold choice in order to guarantee the target $p^{\star}_{\mathrm{FA}}$.

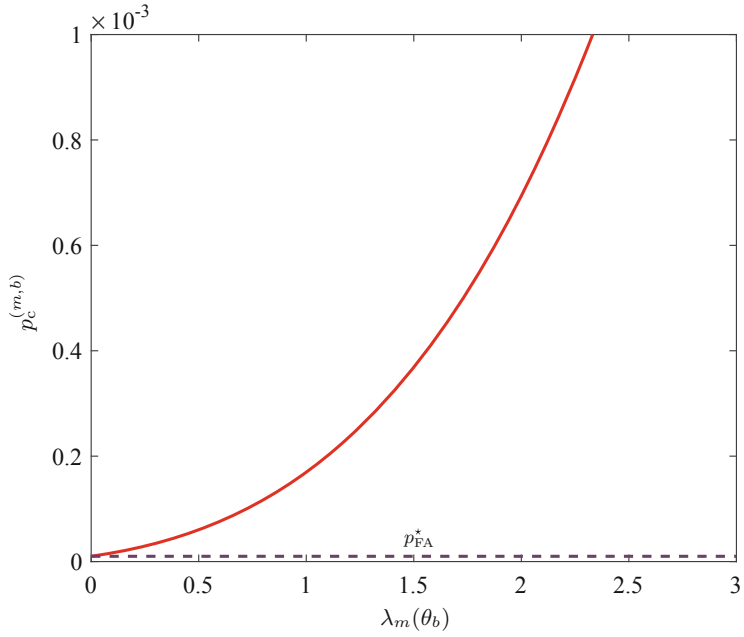

Fig. 4. Bin-crossing probability when the threshold $\tilde{\xi}^{\star}$ of Fig. 3 is adopted.

3.3 Numerical Evaluation of the NCP

Considering the previous results, we now map the obtained non-centrality parameter (NCP) $\lambda_m(\theta_b)$ into possible real values. In particular, we considered a receiver noise figure $F = 4\,\text{dB}$ and $T_0 = 290\,\text{K}$. A simple and practical solution is to consider free-space propagation from the target to the radar section, and to assume the entire backscattered energy contained into one bin, which represents a worst case scenario. Successively, we dimension $\lambda_m(\theta_b)$ according to the expected path-loss of the signal in each bin from a side-lobe direction. We obtained

$$\lambda_m(\theta_b) = 2\gamma_m(\theta_b) = \frac{1}{\sigma^2}\int_W S(f)\cdot G_{\text{sl}}^2(f,\theta_b) M \frac{c^2}{f^2\,(4\pi)^3\,d_m^4} df \tag{17}$$

where M is the target radar cross-section in the side-lobe direction,[3] $G_{\text{sl}}(f,\theta_b)$ is the maximum side-lobe gain in the steering direction θ_b, $S(f)$ is the transmitted power spectral density (PSD) and d_m is the target-array distance. Note that the power spectral density (PSD) has been set so that EIRP, evaluated according to $G_{\max}$, is compliant with the Federal Communications Commission (FCC) regulations. In our scenario we fixed EIRP$= 30\,\text{dBm}$.

As existing antennas, we consider 15×15 massive arrays, which are a possible candidate for this kind of applications thanks to their narrow beam [3], by accounting for a different number of quantization bits which impact in the array pattern. As an example, Table 1 reports different values of $G_{\max}$ and G_{sl} at the central frequency $f_c = 60\,\text{GHz}$.[4] The side lobe level (SLL) represents the difference (in [dB]) between the maximum gain and the peak of the main side lobe G_{sl}.

In Fig. 5, $\lambda_m(\theta_b)$ values are reported according to different quantization bits, the bin index (i.e. the target distance from the TX/RX) and different values of M. Consequently, according to Fig. 4, we found that $\lambda_m(\theta_b)$ is often above 0.2, which was found as a limit value in order to preserve $p_{\text{c}}^{(m,b)} = p_{\text{FA}}^{\star}$ in the

Table 1. SLL and maximum gain at $f_c = 60\,\text{GHz}$ for different phase compensation conditions.

$\theta_b = 0^\circ$			$\theta_b = 20^\circ$		
Quantization	$G_{\max}$ [dBi]	SLL [dB]	Quantization	$G_{\max}$ [dBi]	SLL [dB]
Perfect	27.1	23.3	Perfect	26.8	22.8
3 bits	26.9	24.6	3 bits	26.5	20.7
2 bits	26.4	20.6	2 bits	25.9	19.4
1 bit	23.5	16.8	1 bit	22.2	13.6

[3] Note that here we neglected the dependency of M with the frequency.

[4] The values account also for the spillover loss when massive arrays, such as transmitarrays [2], are excited with an external source.

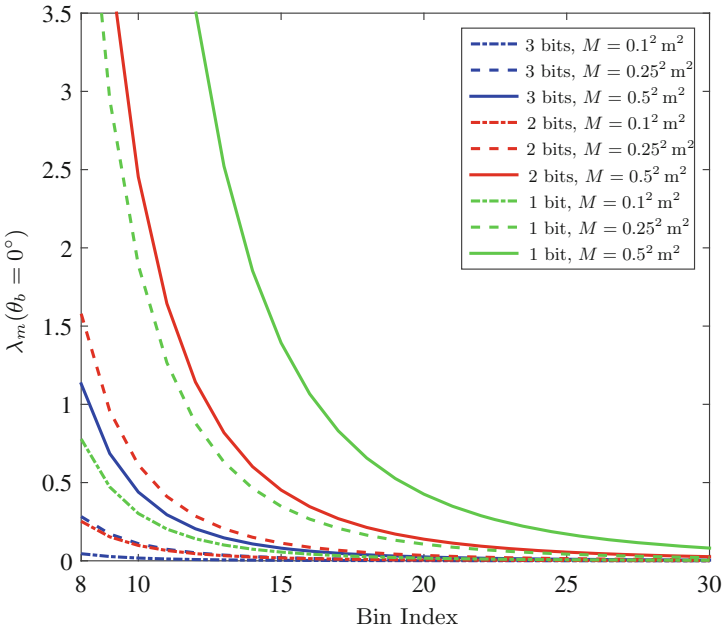

Fig. 5. NCP values for different values of M and for $\theta_b = 0°$.

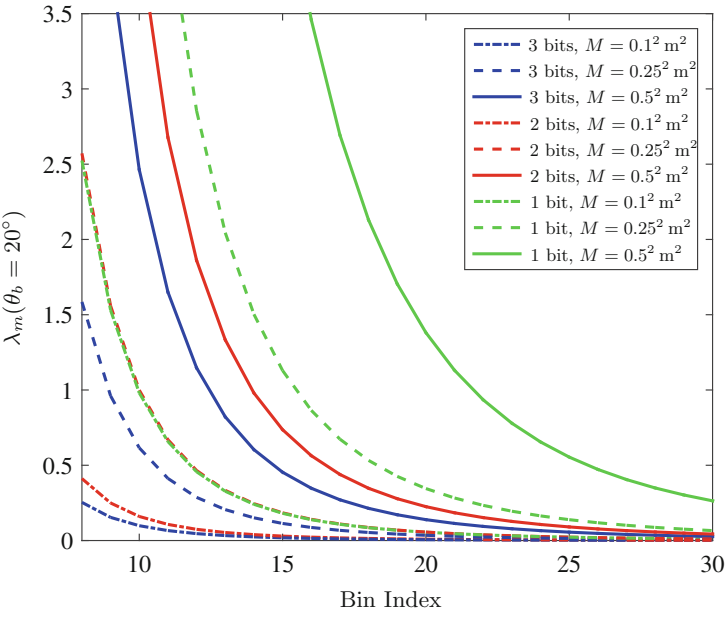

Fig. 6. NCP values for different values of M and for $\theta_b = 20°$.

presence of side-lobes. Note that the values of $\lambda_m(\theta_b)$ are also strictly related to the steering direction. In fact, when electronically beamsteering is performed, the side lobe level (SLL) might increase, as also reported in Table 1. Indeed, also the $\lambda_m(\theta_b)$ values change, as clearly evidenced in Fig. 6, especially when a low number of quantization bits is adopted. This effect suggests that the side lobe level (SLL) should be treated differently for each steering direction, as it is a key design parameter to be taken into account both for the massive array choice and for the threshold evaluation criterion. From one side, in order to reduce the interfering signal coming from directions different from θ_b, it is important to reduce at most the side lobe level (SLL): for example, in our case study, at least 3 quantization bits are required to preserve reliable performance. On the other side, the choice of the massive array could be jointly performed with other operations in order to improve the performance. In fact, different techniques can be adopted in order to counteract side lobes effects on target detection. A possibility could be the adoption of a side-lobe blanker. In particular, a guard channel, which can be omni-directional or adaptive according to the direction, can be implemented to eliminate impulsive interference (hostile or from other neighboring radars) [17,18]. Analogously, in [19], a technique to mitigate the image artifacts due to the sidelobes of the random array is reported. All these solutions are appealing, but they can not be adopted due to their computational complexity and the use of coherent receivers.

A simple and effective solution could be the conception of new threshold design strategies, which accounts for both the receiver noise and the impact of the non-central parameters $\lambda_m(\theta_b)$. Future works will consider a constant false alarm rate (CFAR) approach where the $P_{\mathrm{FA}}^{\star}$ and the different level of interferers per bin are used to properly set the threshold.

4 Conclusions

In this paper we analyzed the impact of massive arrays side-lobes into detection performance for personal radars applications. In particular, in order to keep both the antenna array complexity and the cost low, a discrete set of phase shifts are often adopted for beamforming at the expense of an increased side-lobe level. In these situations, the design of a threshold accounting only for the receiver noise is not sufficient to guarantee the correct functioning of the system in terms of detection performance. In fact, as demonstrated by simulation results, the presence of side-lobes could drastically increase the crossing probability even when there is no target in the steering direction. This effect poses several attentions in the massive array choice according to its maximum side lobe level (SLL). Future studies will investigate the design of a threshold which accounts for the side-lobes effect in each steering direction.

Acknowledgments. This research was supported in part by the IF-EF Marie-Curie project MAPS (Grant 659067) and by the European H2020 project XCycle (Grant 635975).

References

1. Guidi, F., Guerra, A., Dardari, D.: Personal mobile radars with millimeter-wave massive arrays for indoor mapping. IEEE Trans. Mobile Comput. **15**(6), 1471–1484 (2016)
2. Clemente, A., Dussopt, L., Sauleau, R., Potier, P., Pouliguen, P.: Wideband 400-element electronically reconfigurable transmitarray in X band. IEEE Trans. Antennas Propag. **61**(10), 5017–5027 (2013)
3. Guerra, A., Guidi, F., Clemente, A., D'Errico, R., Dussopt, L., Dardari, D.: Application of transmitarray antennas for indoor mapping at millimeter-waves. In: Proceedings of the IEEE European Conference on Networks and Communicationa (EUCNC) (2015)
4. Dissanayake, M.W.M.G., Newman, P., Clark, S., Durrant-Whyte, H., Csorba, M.: A solution to the simultaneous localization and map building (SLAM) problem. IEEE Trans. Robot. Autom. **17**(3), 229–241 (2001)
5. Jose, E., Adams, M.: An augmented state SLAM formulation for multiple line-of-sight features with millimetre wave RADAR. In: Proceedings of the IEEE/RSJ International Conference on Intelligent Robots and System, pp. 3087–3092, Aug 2005
6. Jose, E., Adams, M., Mullane, J., Patrikalakis, N.: Predicting millimeter wave radar spectra for autonomous navigation. IEEE Sens. J. **10**(5), 960–971 (2010)
7. Shen, Y., Win, M.: Fundamental limits of wideband localization; part I: A general framework. IEEE Trans. Inf. Theory **56**(10), 4956–4980 (2010)
8. Rondinelli, L.: Effects of random errors on the performance of antenna arrays of many elements. In: IRE International Convention Record, vol. 7, pp. 174–189 (1959)
9. Ruze, J.: Antenna tolerance theory - A review. Proc. IEEE **54**(4), 633–640 (1966)
10. Urkowitz, H.: Energy detection of unknown deterministic signals. Proc. IEEE **55**(4), 523–531 (1967)
11. Abramowitz, M., Stegun, I.A.: Handbook of Mathematical Functions wih Formulas, Graphs, and Mathematical Tables. United States Department of Commerce, Washington, D.C. (1970)
12. Mariani, A., Giorgetti, A., Chiani, M.: Effects of noise power estimation on energy detection for cognitive radio applications. IEEE Trans. Commun. **59**(12), 3410–3420 (2011)
13. Chiani, M.: Integral representation and bounds for marcum Q-function. IEEE Electr. Lett. **35**(6), 445–446 (1999)
14. Guidi, F., Decarli, N., Bartoletti, S., Conti, A., Dardari, D.: Detection of multiple tags based on impulsive backscattered signals. IEEE Trans. Commun. **62**(11), 3918–3930 (2014)
15. FCC: Federal Communications Commission (FCC), 18–07-0082-01-0000d1, Amendment of Part 15 Rules for License-Exemppt 57–64 GHz Band
16. Slepian, D., Sonnenblick, E.: Eigenvalues associated with prolate spheroidal wave functions of zero order. Bell Sys. Tech. J. **44**, 1745–1758 (1965)
17. Nickel, U.: Detection with adaptive arrays with irregular digital subarrays. In: Proceedings of the IEEE Radar Conference, pp. 635–640, April 2007
18. Richmond, C.: Performance of the adaptive sidelobe blanker detection algorithm in homogeneous environments. IEEE Trans. Sig. Process. **48**(5), 1235–1247 (2000)
19. Tsao, J., Steinberg, B.: Reduction of sidelobe and speckle artifacts in microwave imaging: the CLEAN technique. IEEE Trans. Antennas Propag. **36**(4), 543–556 (1988)